# NiO/ $\beta$ -(Al<sub>x</sub>Ga<sub>1-x</sub>)<sub>2</sub>O<sub>3</sub> /Ga<sub>2</sub>O<sub>3</sub> Heterojunction Lateral Rectifiers with Reverse Breakdown Voltage > 7kV

Running title: NiO/β-(Al<sub>x</sub>Ga<sub>1-x</sub>)<sub>2</sub>O<sub>3</sub> /Ga<sub>2</sub>O<sub>3</sub> Heterojunction Lateral Rectifiers

Running Authors: Wan et al.

Hsiao-Hsuan Wan<sup>1</sup>, Jian-Sian Li<sup>1</sup>, Chao-Ching Chiang<sup>1</sup>, Xinyi Xia<sup>1</sup>, Fan Ren<sup>1</sup>, Hannah N. Masten<sup>2</sup>, James Spencer Lundh<sup>2</sup>, Joseph A. Spencer<sup>3,4</sup>, Fikadu Alema<sup>5</sup>, Andrei Osinsky<sup>5</sup>, Alan G. Jacobs<sup>3</sup>, Karl Hobart<sup>3</sup>, Marko J. Tadjer<sup>3</sup> and S.J. Pearton <sup>6,a)</sup>

<sup>1</sup>Department of Chemical Engineering, University of Florida, Gainesville, FL 32611 USA

<sup>2</sup>National Research Council Postdoctoral Fellow at U.S. Naval Research Laboratory

<sup>3</sup>U.S. Naval Research Laboratory, Washington, DC, USA

<sup>4</sup>Virginia Tech, Blacksburg VA, USA

<sup>5</sup>Agnitron Technology, Inc, Chanhassen, MN, USA

<sup>6</sup> Department of Materials Science and Engineering, University of Florida, Gainesville, FL 32611 USA

a) Electronic mail: spear@mse.ufl.edu

NiO/  $\beta$ -(Al<sub>x</sub>Ga<sub>1-x</sub>)<sub>2</sub>O<sub>3</sub> /Ga<sub>2</sub>O<sub>3</sub> heterojunction lateral geometry rectifiers with diameter 50-100  $\mu$ m exhibited maximum reverse breakdown voltages >7kV, showing the advantage of increasing the bandgap using the  $\beta$ -(Al<sub>x</sub>Ga<sub>1-x</sub>)<sub>2</sub>O<sub>3</sub> alloy. This Si-doped alloy layer was grown by Metal Organic Chemical Vapor Deposition with an Al composition of ~21 %. On state resistances were in the range 50-2180  $\Omega$ .cm<sup>2</sup>, leading to power figures-of-merit up to 0.72 MW.cm<sup>-2</sup>. The forward turn-on voltage was in the range 2.3-2.5 V, with maximum on/off ratios >700 when switching from 5V forward to reverse biases up to -100V. Transmission line measurements showed the specific contact resistance was 0.12  $\Omega$ .cm<sup>2</sup>. The breakdown voltage is among the highest reported for any lateral geometry Ga<sub>2</sub>O<sub>3</sub>-based rectifier.

#### I. INTRODUCTION

There is significant recent interest in development of Ga<sub>2</sub>O<sub>3</sub> power devices due to their capability for high temperature operation, reduced on-state and switching losses due to lower on-resistance for high voltage devices, and potentially higher frequency switching capability (1-8). These are targeted for renewable energy transmission systems, electric vehicle (EV) traction inverter and motor control systems, fast charging stations and more electric aircraft  $^{(9,10)}$ . Since the efficiency of EV powertrain inverters is partially determined by the efficiency of the switching transistors, it is of interest to examine ultrawide-bandgap semiconductor electronics. The successful development of these power transistors is expected to significantly increase the longevity of a battery charge and the resultant cost of an EV. For devices in EV inverter applications, in addition to low switching loss and good thermal capability, high power and good robustness are highly desirable. In addition, the currently used passive and active filtering used to mitigate switching transients on motor drive systems in electro-hydrostatic and electromechanical actuators for air platforms could be replaced by optically-gated power semiconductor devices (11). The absence of a native p-type doping capability has led to use p-type oxides such as Cu<sub>2</sub>O <sup>(12)</sup> or NiO <sup>(13-17)</sup> in heterojunctions with n-type Ga<sub>2</sub>O<sub>3</sub>.

An additional advance comes from use of the wider bandgap alloy  $(Al_xGa_{1-x})_2O_3$  in place of  $Ga_2O_3$ .  $(Al_xGa_{1-x})_2O_3$  alloys with compositions up to x = 40% have been grown with good crystalline quality on (010)-oriented  $\beta$ -Ga<sub>2</sub>O<sub>3</sub> substrates, and  $x \ge 50\%$  can be obtained on (100) and (-201)  $\beta$ -Ga<sub>2</sub>O<sub>3</sub> substrates when the layers are grown by Metal Organic Chemical Vapor Deposition (MOCVD) (18-23). Phase pure  $\beta$ -

(Al<sub>x</sub>Ga<sub>1-x</sub>)<sub>2</sub>O<sub>3</sub> films with Al content up to 27% have been grown with this technique <sup>(21-23)</sup>, which is promising from the viewpoint that this is the standard epitaxial growth method for most compound semiconductors. While most Ga<sub>2</sub>O<sub>3</sub>-based rectifiers to date have been vertical geometry to increase the current-carrying capability <sup>(24-32)</sup>, there is also interest in lateral geometry devices <sup>(33)</sup>, whose breakdown voltage can be more easily scaled by increasing the contact separation distance. Sundaram et al. <sup>(20)</sup> showed that addition of a 30 nm-thick  $\beta$ -(Al<sub>0.22</sub>Ga<sub>0.78</sub>)<sub>2</sub>O<sub>3</sub> cap to an n-type  $\beta$ -Ga<sub>2</sub>O<sub>3</sub> layer grown by metal organic chemical vapor deposition increased the breakdown voltage. The cap increased the surface Schottky barrier with Pt metal, resulting in reduced carrier injection under reverse bias. Masten et al. <sup>(19)</sup> reported  $\beta$ -(Al<sub>x</sub>Ga<sub>1-x</sub>)<sub>2</sub>O<sub>3</sub>/ $\beta$ -Ga<sub>2</sub>O<sub>3</sub> heterostructure MESFETs with on/off current ratio ~300 and rain current of 1.8 mA/mm at a gate bias of 5 V and drain bias of 30 V.

In this paper, we demonstrate breakdown voltages > 7kV in lateral NiO/ $\beta$ - $(Al_xGa_{1-x})_2O_3$  / $Ga_2O_3$  heterojunction rectifiers, with the basic layer structure grown by MOCVD, with the bilayer NiO deposited by sputtering. The devices show promising on/off ratio and low Ohmic contact resistance.

## II. EXPERIMENTAL

The β-(Al<sub>x</sub>Ga<sub>1-x</sub>)<sub>2</sub>O<sub>3</sub>/β-Ga<sub>2</sub>O<sub>3</sub> heterostructures were grown in an Agnitron Agilis 500 MOCVD reactor with trimethylaluminum (TMAl), triethylgallium (TEGa), and oxygen (5N) as precursors, and argon (6N) as carrier gas <sup>(19, 20)</sup>. The TMAl and TEGa precursors were used to grow 70 nm thick Si doped β-(Al<sub>x</sub>Ga<sub>1-x</sub>)<sub>2</sub>O<sub>3</sub> layer on ~300 nm UID β-Ga<sub>2</sub>O<sub>3</sub> buffer layer, respectively, on a Fe doped (010) β-Ga<sub>2</sub>O<sub>3</sub> 1" substrate (Synoptics). The

AlGaO layer was Si-doped using silane diluted in nitrogen (SiH<sub>4</sub>/N<sub>2</sub>) as the source with the targeted doping concentration of  $\sim 4 \times 10^{17}$  cm<sup>-3</sup>. The growth pressure was 15 Torr, and the growth temperature was 800°C, while the oxygen flow rate for the growth of the AlGaO was 600 sccm. The gas phase [TMAl]/([TMAl]+[TEGa]) molar flow rate ratio was  $\sim 8.4\%$ , producing an Al concentration of 20.6% calculated from X-ray diffraction (XRD). Room temperature Hall measurements showed a sheet resistance of  $R_{\rm SH} = 7636$   $\Omega/{\rm sq.}$ , with a sheet carrier concentration of 7.2 x  $10^{12}$  cm<sup>-2</sup> and associated electron mobility of 114 cm<sup>2</sup>/V·s. It should be noted that the unintentionally doped buffer is also somewhat conductive, around  $10^{15}$  cm<sup>-3</sup>, so the Hall measurements do not isolate the transport properties of the doped AlGaO layer.

The NiO bilayer was deposited on top of the epi layer by magnetron sputtering from dual NiO targets at 3mTorr and 150W of 13.56 MHz power. We used two targets to increase the deposition rate to  $\sim 0.2$  Å.sec<sup>-1</sup>. The Ar/O<sub>2</sub> gas ratio during sputtering was used to control the doping in the NiO in the range  $2 \times 10^{18}$ -  $2 \times 10^{19}$  cm<sup>-3</sup>, with mobility < 1 cm<sup>2</sup>·V<sup>-1</sup> s<sup>-1</sup>. The bandgap was 3.8 eV, consistent with literature values <sup>(34)</sup>. We employed a bilayer of NiO of two different doping levels to both increase breakdown voltage and obtain low sheet resistance The band alignment for the NiO on  $Ga_2O_3$  is type II, staggered gap, allowing facile transport of holes across the heterojunction <sup>(35)</sup>. The front-side of the device structure was contacted by 100 nm of Ni/Au metal, with circular contacts of 50-100  $\mu$ m. Ohmic contacts to the lateral rectifier structure were made by 100nm of Ti/Au. A schematic is shown in Figure 1(a), while the different size rectifiers and the Transmission Line Measurement (TLM) pattern used to extract contact resistance is shown in Figure 1(b).

The current-voltage (I-V) characteristics were recorded on a Tektronix 371-B curve tracer at high voltage while an Agilent 4156C was used for forward and reverse current measurements at low biases. The reverse breakdown voltage was defined as the bias for a reverse current density reaching 0.1 A.cm<sup>2</sup>.

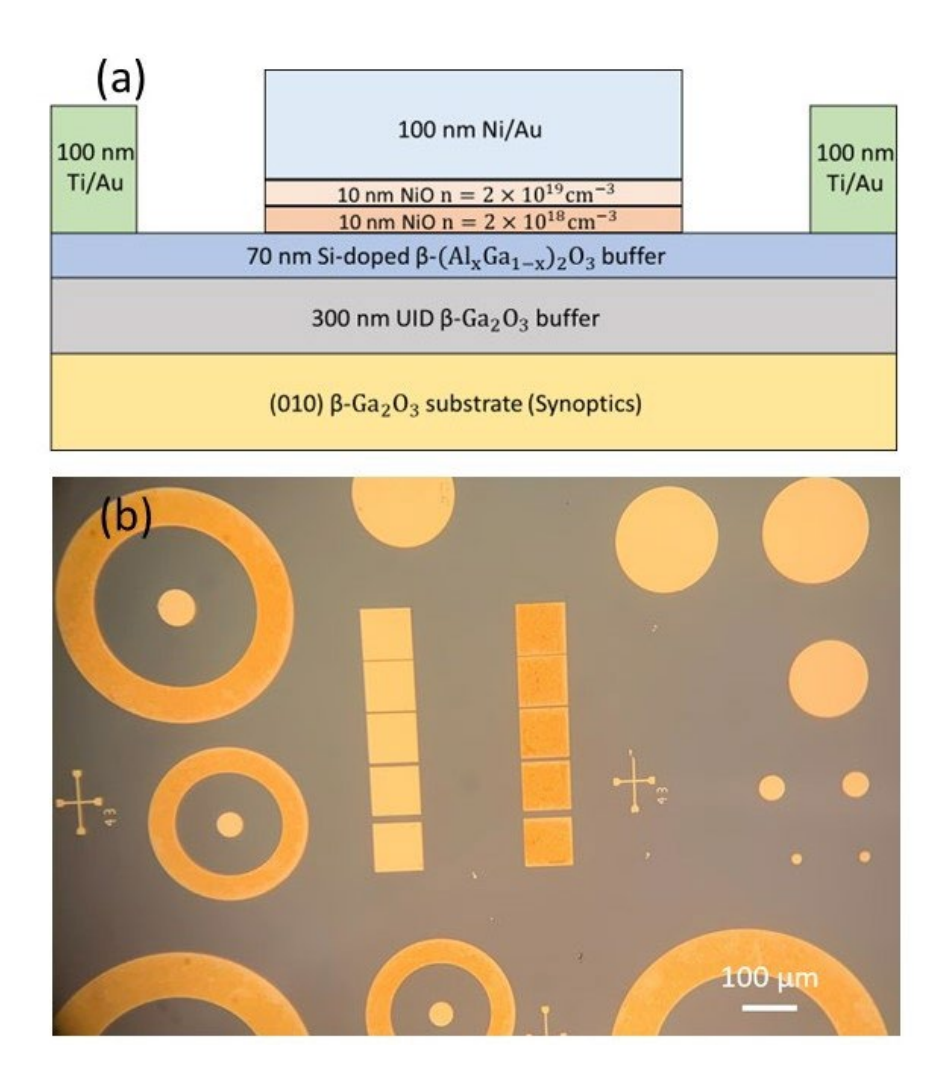


Fig. 1. (a) Schematic of lateral diode (b) Optical image of diodes and contact metals for TLM measurement.

# **III. RESULTS AND DISCUSSION**

The TLM data for the structure is shown in Figure 2. The specific contact resistance was  $0.12~\Omega.\text{cm}^2$ , with a transfer length of  $1.48~\mu\text{m}$ . The sheet resistance under the Ohmic contact was  $5.3 \times 10^6~\Omega/\text{square}$ , with a total resistance of  $8.1~\text{k}\Omega.\text{mm}$ . These are reasonable values given the low doping in the wide bandgap (Al<sub>x</sub>Ga<sub>1-x</sub>)<sub>2</sub>O<sub>3</sub> alloy.

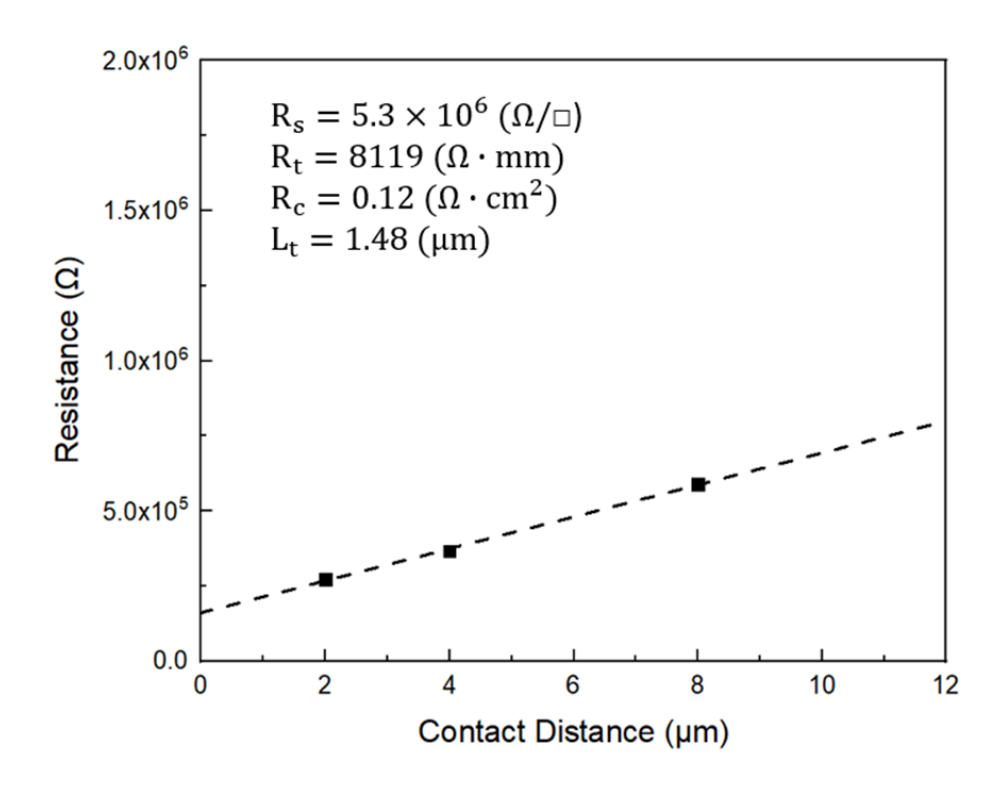


Fig. 2. TLM measurement data, showing the parameters extracted from the plot of resistance as a function of contact distance.

Figure 3 shows the forward current density characteristics and associated on-state resistances, R<sub>ON</sub>, for three different rectifier diameters. The power figure-of-merit (FOM), V<sub>B</sub><sup>2</sup>/R<sub>ON</sub>, where V<sub>B</sub> is the reverse breakdown voltage, for the 50μm rectifier was 0.01 MW.cm<sup>-2</sup>, for 75μm was 0.34 MW.cm<sup>-2</sup>, while for 100μm, FOM was 0.72 MW.cm<sup>-2</sup>. These are well below the values for vertical geometry NiO/ Ga<sub>2</sub>O<sub>3</sub> rectifiers because of the higher on-state resistance in lateral devices (14-16). The forward current was still dominated by thermionic emission current.

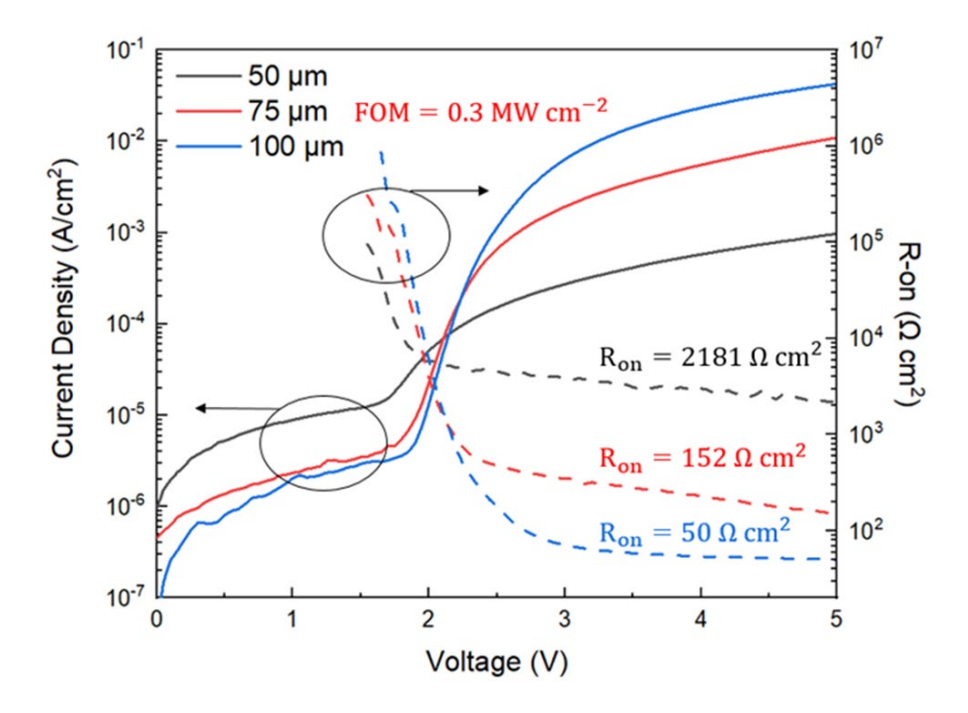


Fig. 3. Forward current density and on-state resistance for rectifiers of three different diameters.

Figure 4 shows linear plots of forward current to extract the forward turn-on voltage. This was in the range 2.3-2.5, consistent with previous reports for NiO/Ga<sub>2</sub>O<sub>3</sub> rectifiers and demonstrating that the inclusion of the alloy did not degrade the turn-on voltage to a significant degree <sup>(15-17)</sup>.

The breakdown voltages were extracted from the reverse I-V characteristics, as shown in Figure 5. The maximum value we obtained was over 7kV. This is the highest reported value for a lateral Ga<sub>2</sub>O<sub>3</sub> rectifier. Bhattacharya et al.<sup>(36)</sup> reported 4.4 kV breakdown in Ga<sub>2</sub>O<sub>3</sub> metal semiconductor (MESFETs), while values <4kV are reported for MESFETs and MOSFETs <sup>(37-40)</sup>. The highest breakdown voltage for a lateral MOSFET is 8.56MV for 60 µm gate-drain separation, obtained after vacuum annealing and slightly higher than unannealed devices <sup>(41,42)</sup>.

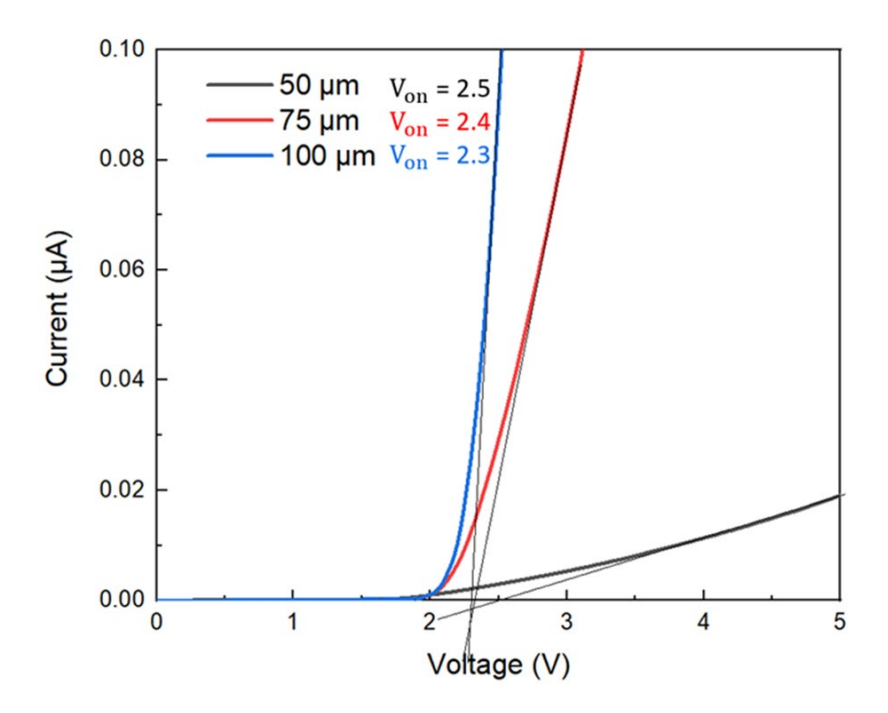


Fig. 4. Forward turn-on voltage for the three rectifier different diameters.

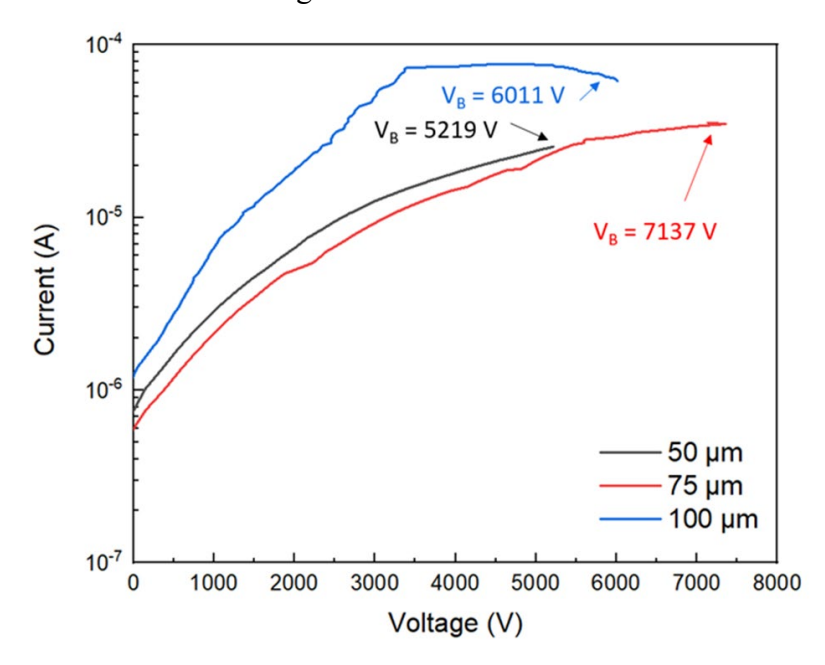


Fig. 5. Reverse I-V characteristics of rectifiers of three different diameters, showing the associated breakdown voltages.

A more detailed view of the reverse current at low biases, up to -100V, is shown in Figure 6. This reverse leakage current was dominated by thermionic field

emission (TFE) in this bias range. At  $> \sim 300$ V, electron injection into the drift region produced an I  $\propto$  V<sup>n</sup> relationship, where n<2. This is typical of trap-assisted space-charge-limited conduction.

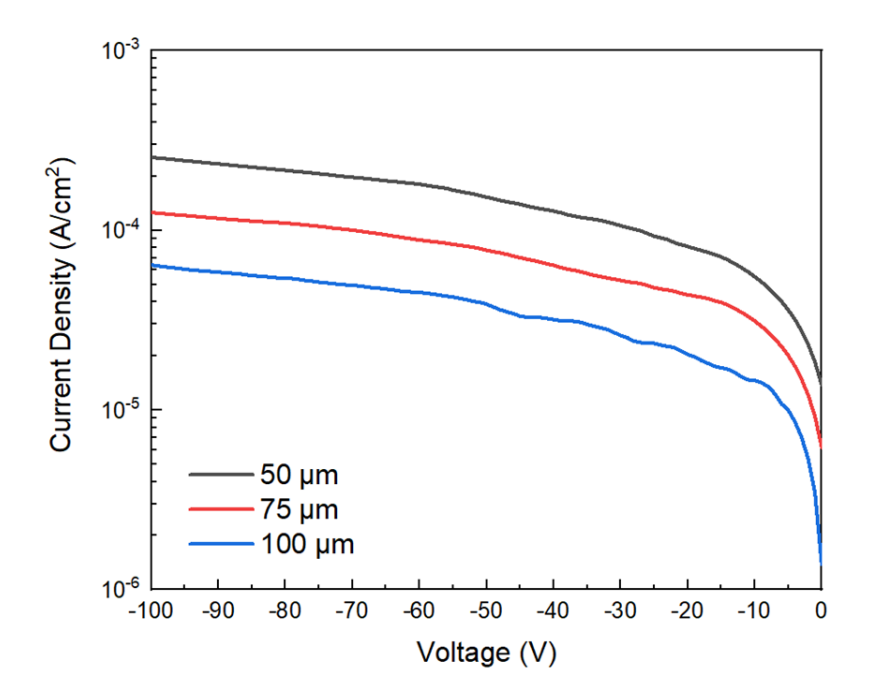


Fig. 6. Reverse I-V characteristics at low biases.

Figure 7 shows the diode on-off ratio for the NiO/ Ga<sub>2</sub>O<sub>3</sub> heterojunction rectifiers when switching from -5V forward voltage to reverse voltages shown on the x-axis, ie. up to 100V. The maximum on/off ratio was >700.

To put the results in context, Figure 8 shows a compilation of reported breakdown voltages and on-state resistances from different institutions <sup>(38-42)</sup>. The device types are mainly either MESFETs or various types of MOSFET geometries, which we have included under the general heading of lateral FETs. Our results are among the highest figures of merit for lateral Ga<sub>2</sub>O<sub>3</sub> devices, showing the advantage of both the ternary alloy to increase bandgap and the use of the NiO-(Al<sub>0.21</sub> Ga<sub>0.79</sub>)<sub>2</sub>O<sub>3</sub> p-n heterojunction. Since both switching devices and rectifiers are needed for inverter

systems, it is worth developing both lateral and vertical geometry devices in this ultrawide bandgap materials system. The clear need is to lower the on-state resistance, while retaining the high breakdown voltages in our devices. Note that all of the reported figures of merit for lateral devices fall well short of the theoretical values for Ga<sub>2</sub>O<sub>3</sub>, with only some being superior at this stage to the limits for Si. This emphasizes how much more development is needed for Ga<sub>2</sub>O<sub>3</sub> power electronics.

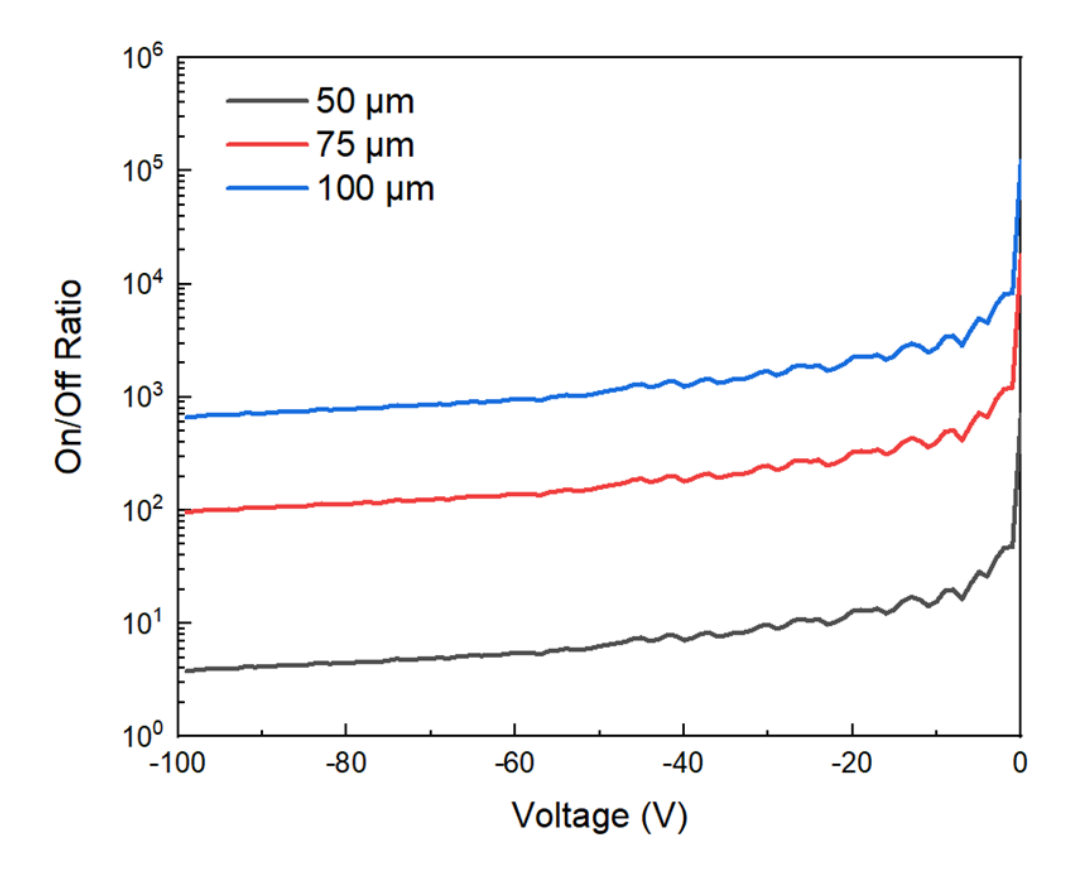


Fig 7. On/off ratio when switching from -5V to the value shown on the x-axis for three different diameter rectifiers.

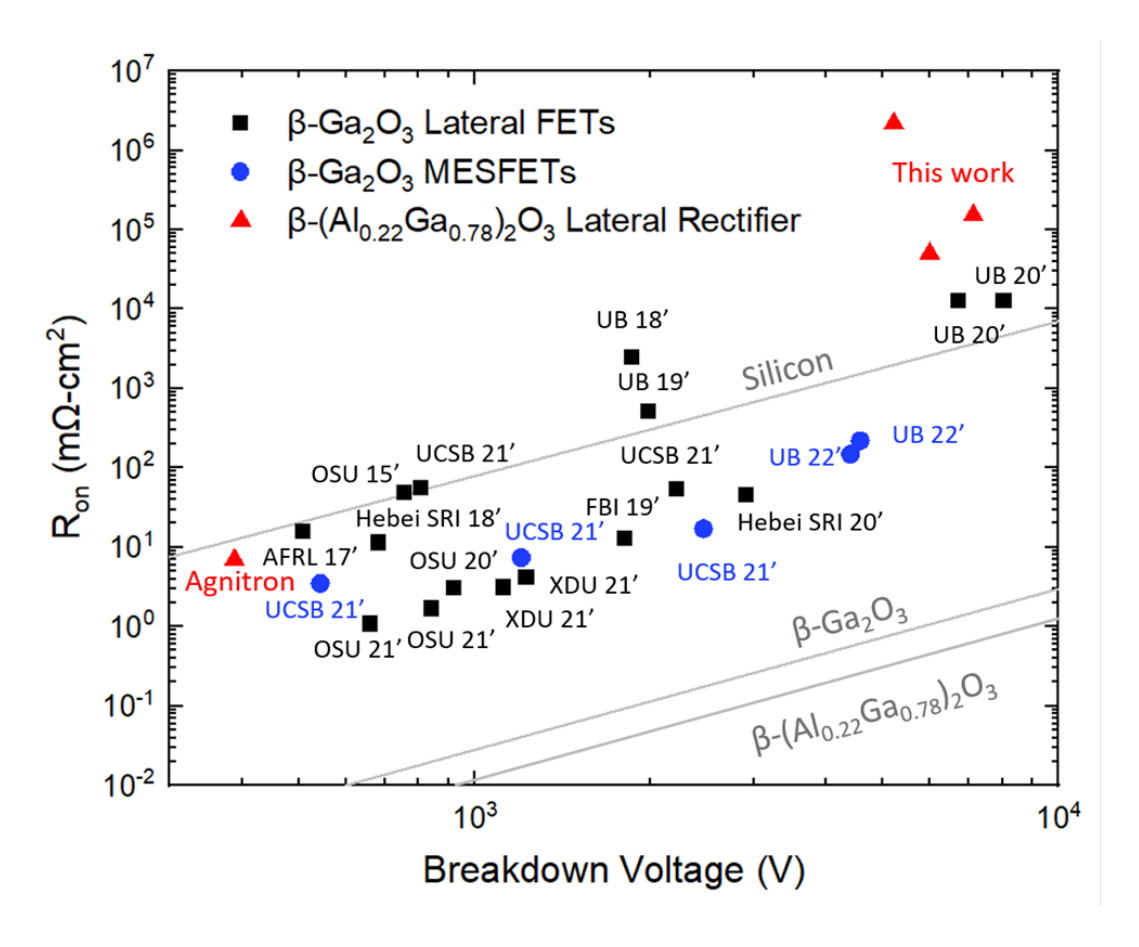


Fig. 8. Compilation of reported R<sub>on,sp</sub> - V<sub>BR</sub> values for lateral geometry Ga<sub>2</sub>O<sub>3</sub> based devices. The previously reported values come from references 38-42.

# IV. SUMMARY AND CONCLUSIONS

Promising performance from NiO/ $\beta$ -(Al<sub>x</sub>Ga<sub>1-x</sub>)<sub>2</sub>O<sub>3</sub>/Ga<sub>2</sub>O<sub>3</sub> heterojunction lateral geometry rectifiers was obtained, with maximum reverse breakdown voltage > 7kV. This is the highest reported for lateral rectifiers and shows the value of both the NiO gate structure and the inclusion of the wider band gap of the  $\beta$ -(Al<sub>x</sub>Ga<sub>1-x</sub>)<sub>2</sub>O<sub>3</sub> alloy. It is not expected there is significant leakage conduction contribution from the NiO layer due to formation of polarons in this material <sup>(43-46)</sup>, making this a good choice as the p-side of the heterojunction. The use of the industry standard MOCVD growth, simple fabrication

and avoidance of mesa etching processes are all advantages of the approach outlined in this work.

## **ACKNOWLEDGMENTS**

Work performed as part of Interaction of Ionizing Radiation with Matter University Research Alliance (IIRM-URA), sponsored by the Department of the Defense, Defense Threat Reduction Agency under award HDTRA1-20-2-0002. The content of the information does not necessarily reflect the position or the policy of the federal government, and no official endorsement should be inferred. The work was also supported by NSF DMR 1856662 (James Edgar). The authors thank the staff of the Nanoscale Research Facility at UF, part of the Herbert Wertheim College of Engineering's Research Service Centers (RSC) for assistance in device fabrication. H.N.M. and J.S.L acknowledge postdoctoral funding from the National Research Council, Washington DC. Fabrication equipment and support was provided by the NRL Nanoscience Institute and Dr. Brian Downey (NRL). The authors acknowledge Dr. John Blevins (AFRL) for providing Ga<sub>2</sub>O<sub>3</sub> substrates for this work. Agnitron's ongoing β-Ga<sub>2</sub>O<sub>3</sub> development work is in part supported by ONR contract number N6833518C0192, under the direction of Mr. Lynn Petersen, and AFOSR contract number FA9550-17-P-0029, under the direction of Dr. Ali Sayir. Research at the Naval Research Laboratory was supported by the Office of Naval Research.

# **AUTHOR DECLARATIONS**

#### **Conflicts of Interest**

The authors have no conflicts to disclose

## DATA AVAILABILITY

The data that supports the findings of this study are available within the article.

## **REFERENCES**

<sup>1</sup> Marko Tadjer, Science, 378, 6621 (2022).

<sup>2</sup>S. J. Pearton, J. Yang, P.H. Cary IV, F. Ren, J. Kim, M.J. Tadjer and M.A. Mastro., Appl. Phys. Rev. 5, 011301 (2018).

<sup>3</sup>P. Dong, Jincheng Zhang, Qinglong Yan, Zhihong Liu, Peijun Ma, Hong Zhou and Yue Hao, IEEE Electr Device L, 43, 765 (2022).

<sup>4</sup>E. Chikoidze, C. Sartel, H. Mohamed, I. Madaci, T. Tchelidze, M. Modreanu, P. Vales-Castro, C. Rubio, C. Arnold, V. Sallet, Y. Dumont, and A. Perez-Tomas, J. Mater Chem C7, 10231 (2019).

<sup>5</sup>Yuangang Wang, Hehe Gong, Yuanjie Lv, Xingchang Fu, Shaobo Dun, Tingting Han, Hongyu Liu, Xingye Zhou, Shixiong Liang, Jiandong Ye, Rong Zhang, Aimin Bu, Shujun Cai and Zhihong Feng, IEEE T. Power Electr. 37, 3743 (2022).

<sup>6</sup>Elaheh Ahmadi, and Yuichi Oshima, J. Appl. Phys. 126, 160901 (2019).

<sup>7</sup>S.J. Pearton, Fan Ren, Marko Tadjer and Jihyun Kim, J. Appl. Phys. 124, 222901 (2018).

<sup>8</sup>Jincheng Zhang, Pengfei Dong, Kui Dang, Yanni Zhang, Qinglong Yan, Hu Xiang, Jie Su, Zhihong Liu, Mengwei Si, Jiacheng Gao, Moufu Kong, Hong Zhou and Yue Hao, Nat Commun 13, 3900 (2022).

<sup>9</sup>A.J. Wileman, Sohaib Aslam, Suresh Perinpanayagam, Prog Aerosp. Sci., 127, 100739 (2021).

<sup>10</sup>Jin Wang, IEEE Power Electr. M. 9, 16 (2022)

<sup>11</sup>J. S. Sullivan, "Wide Bandgap Extrinsic Photoconductive Switches, "Lawrence Livermore National Laboratory Report LL LLNL-TH-523591, January 20, 2012.

<sup>12</sup>Tatsuro Watahiki, Yohei Yuda, Akihiko Furukawa, Mikio Yamamuka, Yuki Takiguchi, and Shinsuke Miyajima, Appl. Phys. Lett. 111, 222104 (2017).

- <sup>13</sup>J. Zhang, S. Han, M. Cui, X. Xu, W. Li, H. Xu, C. Jin, M. Gu, L. Chen and K.H. L. Zhang, ACS Appl. Electron. Mater. 2, 456 (2020).
- <sup>14</sup>Y. Lv, Y. Wang, X. Fu, Shaobo Dun, Z. Sun, Hongyu Liu, X. Zhou, X. Song, K. Dang, S. Liang, J. Zhang, H. Zhou, Z. Feng, S. Cai and Yue Hao, IEEE T. Power Electr. 36, 6179 (2021).
- <sup>15</sup>H. H. Gong, X. H. Chen, Y. Xu, F.-F. Ren, S. L. Gu and J. D. Ye, Appl. Phys. Lett., 117, 022104 (2020).
- <sup>16</sup>F. Zhou, Hehe Gong, Weizong Xu, Xinxin Yu, Yang Xu, Yi Yang, Fang-fang Ren, Shulin Gu, Youdou Zheng, Rong Zhang, Jiandong Ye and Hai Lu, IEEE T. Power Electr, 37, 1223 (2022).
- <sup>17</sup>Jian-Sian Li, Chao-Ching Chiang, Xinyi Xia, Fan Ren, Honggyu Kim and S.J. Pearton, Appl. Phys. Lett.121, 042105 (2022).
- <sup>18</sup>A. F. M. A. U. Bhuiyan, Z. Feng, J. M. Johnson, Z. Chen, H. Huang, J. Hwang, and H. Zhao, Appl. Phys. Lett. 115, 120602 (2019).
- <sup>19</sup>Demonstration of MOCVD Si-doped β-(AlxGa1-x)2O<sub>3</sub> Recessed-Gate MESFET", Hannah N. Masten, James Spencer Lundh, Joseph A. Spencer, Fikadu Alema, Andrei Osinsky, Alan G. Jacobs, Karl D. Hobart, Marko J. Tadjer, presented at IWGO 2022, Japan, October 2022 <sup>20</sup>Prakash P. Sundaram, Fikadu Alema, Andrei Osinsky, and Steven J. Koester, J. Vac. Sci. Technol. A 40, 043211 (2022).
- <sup>21</sup>A. F. M. A. U. Bhuiyan, Z. Feng, H. Huang, L. Meng, J. Hwang, and H. Zhao, J. Vac. Sci. Technol. A 39, 063207 (2021).
- <sup>22</sup>A. F. M. A. U. Bhuiyan, Z. Feng, J. M. Johnson, H. Huang, J. Hwang, and H. Zhao, Appl. Phys. Lett. 117, 142107 (2020).
- <sup>23</sup>G. Seryogin, F. Alema, N. Valente, H. Fu, E. Steinbrunner, A. T. Neal, S. Mou, A. Fine, and A. Osinsky, Appl. Phys. Lett. 117, 262101 (2020).
- <sup>24</sup>K. Konishi, K. Goto, H. Murakami, Y. Kumagai, A. Kuramata, S. Yamakoshi, and M. Higashiwaki, Appl. Phys. Lett. 110, 103506 (2017).
- <sup>25</sup>K. Sasaki, D. Wakimoto, Q. T. Thieu, Y. Koishikawa, A. Kuramata, M. Higashiwaki, and S. Yamakoshi, IEEE Electr Device L. 38, 783 (2017).
- <sup>26</sup>J. Yang, F. Ren, M. Tadjer, S. J. Pearton, and A. Kuramata, ECS J. Solid State SC. 7, Q92 (2018).
- <sup>27</sup>J. Yang, F. Ren, Y. T. Chen, Y. T. Liao, C. W. Chang, J. Lin, M. J. Tadjer, S. J. Pearton, and A. Kuramata, IEEE J. Electron Devi. 7, 57 (2019).

- <sup>28</sup>Z. Hu, H. Zhou, K. Dang, Y. Z. Cai Feng, Y. Gao, Q. Feng, J. Zhang, and Y. Hao, IEEE J. Electron Devi. 6, 815 (2018).
- <sup>29</sup>C. Joishi, S. Rafique, Z. Xia, L. Han, S. Krishnamoorthy, Y. Zhang, S. Lodha, H. Zhao, and S. Rajan, Appl. Phys. Express 11, 031101 (2018).
- <sup>30</sup>W. Li, K. Nomoto, Z. Hu, D. Jena, and H. G. Xing, IEEE Electr. Device L., 41, 107 (2020).
- <sup>31</sup>M. Ji, Neil R. Taylo, Ivan Kravchenko, Pooran Joshi, Tolga Aytug, Lei R. Cao, M. Parans Paranthaman, IEEE T. Power Electr., 36, 41 (2021).
- <sup>32</sup>Ming Xiao, Boyan Wang, Jingcun Liu, Ruizhe Zhang, Zichen Zhang, Chao Ding, Shengchang Lu, Kohei Sasaki, Guo-Quan Lu, Cyril Buttay, and Yuhao Zhang, IEEE T. Power Electr.36,8565 (2021).
- <sup>33</sup>W. Xiong, Xuanze Zhou, Guangwei Xu, Member, IEEE, Qiming He, Guangzhong Jian, Chen Chen, Yangtong Yu, Weibing Hao, Xueqiang Xiang, Xiaolong Zhao, Wenxiang Mu, Zhitai Jia, Xutang Tao and Shibing Long, IEEE Electr Device L, 42, 430 (2021).
- <sup>34</sup>Joseph A. Spencer, Alyssa L. Mock, Alan G. Jacobs, Mathias Schubert, Yuhao Zhang, and Marko J. Tadjer, Appl. Phys. Rev. 9, 011315 (2022).
- <sup>35</sup>Xinyi Xia, Jian Sian Li, Chao Ching Chiang, Timothy Jinsoo Yoo, Fan Ren, Honggyu Kim and S.J. Pearton, J. Phys. D. Appl. Phys. 55, 385105 (2022).
- <sup>36</sup>Arkka Bhattacharyya, Shivam Sharma, Fikadu Alema, Praneeth Ranga, Saurav Roy, Carl Peterson, Geroge Seryogin, Andrei Osinsky, Uttam Singisetti and Sriram Krishnamoorthy, Appl. Phys. Express 15, 061001 (2022).
- <sup>37</sup>Y. Lv, Hongyu Liu, Xingye Zhou, Yuangang Wang, Xubo Song, Yuncong Cai, Qinglong Ya, Chenlu Wang, Shixiong Liang, Jincheng Zhang, Zhihong Feng, Hong Zho, Shujun Cai, and Yue Hao, IEEE Electr Device L., 41, 537 (2020).
- <sup>38</sup>A. Bhattacharyya, Praneeth Ranga, Saurav Roy, Carl Peterson, Fikadu Alema, George Seryogin, Andrei Osinsky, and Sriram Krishnamoorthy, IEEE Electr Device L, 42, 1272 (2021).
- <sup>39</sup>Ke Zeng, Abhishek Vaidya, and Uttam Singisetti, IEEE Electr Device L., 39, 1385 (2018).
- <sup>40</sup>K. Tetzner, Eldad Bahat Treidel, Oliver Hilt, Andreas Popp, Saud Bin Anooz, Günter Wagner, Andreas Thies, Karina Ickert, Hassan Gargouri, and Joachim Würf, IEEE Electr Device L., 40, 1503 (2019).
- <sup>41</sup>Shivam Sharma, Lingyu Meng, A F M Anhar Uddin Bhuiyan, Zixuan Feng, David Eason, Hongping Zhao, and Uttam Singisetti, "Vacuum annealed β-Ga<sub>2</sub>O<sub>3</sub> recess channel MOSFETs

with 8.56 kV Breakdown Voltage," IEEE Electr Device L, (in press, 2022), doi: 10.1109/LED.2022.3218749.

<sup>&</sup>lt;sup>42</sup>S. Sharma, K. Zeng, S. Saha, and U. Singisetti, IEEE Electr Device L. 41, 836 (2020).

<sup>&</sup>lt;sup>43</sup>R. Karsthof, M. Grundmann, A. M. Anton, and F. Kremer, Phys. Rev. B 99, 235201 (2019).

<sup>&</sup>lt;sup>44</sup>G. Geneste, B. Amadon, M. Torrent, and G. Dezanneau, Phys. Rev. B 96, 134123 (2017).

<sup>&</sup>lt;sup>45</sup>K. Jung, H. Seo, Y. Kim, H. Im, J. Hong, J.-W. Park, and J.-K. Lee, Appl. Phys. Lett. 90, 052104 (2007).

<sup>&</sup>lt;sup>46</sup>Yue-Hua Hong, Xue-Feng Zheng, Yun-Long He, Hao Zhang, Zi-Jian Yuan, Xiang-Yu Zhang, Fang Zhang, Ying-Zhe Wang, Xiao-Li Lu, Wei Mao, Xiao-Hua Ma and Yue Hao, Appl. Phys. Lett. 121, 212102 (2022).